DEFORMATION IMAGING OF NONINDUCED DOG TUMOR LESIONS DURING FREEHAND SCANNING

E. Brusseau[1], J.-F. Deprez[1], F. Duboeuf[1], F. Rigout-Paulik[2] and O. Basset[1]

[1] CREATIS; INSA-Lyon; Université Lyon 1; CNRS UMR 5220-Inserm U630; F-69621, France.
[2] Ecole Nationale Vétérinaire de Lyon, France.

ABSTRACT

This paper deals with strain estimation methods used in ultrasound elastography. We recently developed a 2D locally regularized strain estimation technique, which has already been tested with healthy bovine liver samples containing artificial lesions made of agar gel. In this study, we investigated the potential of our method to image the deformation of noninduced (natural) dog tumor lesions during freehand scanning.

Index Terms— Acoustics, Medical imaging, Image processing.

1. INTRODUCTION

Since the very first study conducted by Ophir's group in 1991 [1], static ultrasound elastography has emerged as a valuable technique for tissue characterization. Elastography is an ultrasound-based imaging tool, dedicated to the investigation of local elastic properties of soft biological tissues. This information is relevant for clinical diagnosis since the development of a pathology often induces local variations in tissue stiffness. As an example, breast cancers are typically hard nodules surrounded by softer healthy tissues [2]. Local elasticity properties can be accessed by imaging the medium deformation under compression, since soft areas deform more than harder ones under the same load. In practical terms, ultrasound radiofrequency (RF) images are acquired at different tissue compression levels (Fig.1). Internal displacements and strains are then locally estimated by partitioning the ultrasound data into many overlapping regions of interest (ROI) and by evaluating, for each ROI, the variations induced by the compression.

Until recently, the strain estimation methods used in elastography were mainly 1D. These techniques assume that compression induces tissue local displacements, that occur exclusively along the axial direction. They therefore compute local strains by analyzing these axial variations within signal segments (1D ROI). Such methods are very limited because soft tissues are mainly composed of water, and their axial compression also results in lateral and azimuthal expansions. Accurately estimating the medium's strain should take into account the 3D internal tissue motion. However, since clinical ultrasound scanners mainly provide images, we have investigated the problem of 2D strain estimation from 2D RF data. Most of the 2D techniques reported in the literature assume that with compression the tissue is subjected to internal displacements, locally modeled as a 2D shift of each ROI [3-4]. They then compute strain estimates as the displacement gradient. These methods are interesting, but they lack accuracy with increasing strains because they ignore the variations in shape (comparable to scaling factors) of the postcompression signals, within the ROIs [5]. With the aim of compensating for echo correlation loss, introducing a global regularization into the motion estimation process was proposed [4]. Finally, a method that estimates strain parameters as axial and lateral scaling factors has been introduced [6]. The authors underline that, prior to the strain parameter estimation, the 2D shift that inherently occurs between the initial and compressed ROIs needs to be removed. This compensation uses correlation techniques and may therefore be inaccurate over highly strained regions and consequently corrupt the estimation.

We have recently developed a 2D locally regularized strain estimation technique [7], validated with simulations and tested with *in vitro* healthy biological tissues, into which an artificial lesion made of agar was inserted. In this study, we investi-

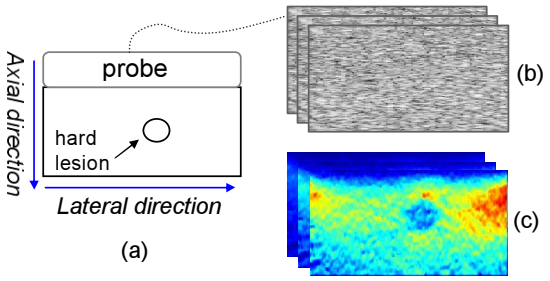

Fig. 1. Elastography principle. (a) Let us consider a medium to be investigated, in this case a parallelepipedic phantom containing a harder spherical inclusion. (b) Several ultrasound RF images are acquired while compressing the medium. Compression-induced signal variations are then analyzed to produce the deformation images (c). Note that in the images acquired, the vertical axis along the ultrasound's beam propagation axis is termed the axial direction while the perpendicular axis corresponds to the lateral direction.

gate the potential of our technique to image the deformation of noninduced (natural) dog tumor lesions during freehand scanning.

2. METHOD

Contrary to most 2D techniques that model the compression-induced local displacement as a 2D shift, we propose a direction-dependent model of tissue motion and deformation, linked to the highly anisotropic character of RF ultrasound image resolution. Let us denote I_1 and I_2 the RF images acquired before and after we compress the medium, respectively. And let R_1 be a specific ROI in I_1 and R_2 its deformed version in I_2. As previously mentioned, in a first approximation, the compression-induced motion can be described locally through a linear transformation:

$$I_2(\alpha x + \tau, \beta y + u) = I_1(x, y) \tag{1}$$

where x and y are the spatial variables, in the axial and lateral directions, τ and u the axial and lateral shifts and α and β the axial and lateral scaling factors, respectively. Equation 1 can be interpreted as follows: for any ROI R_1 in I_1, the medium compression produces a deformation of this ROI (described by the scaling factors) as well as a variation in its position (represented by the 2D shift) induced by the deformation of surrounding tissues. However, in ultrasound RF images the lateral resolution is much coarser than the axial one, making the estimation of a scaling factor difficult. For this reason, β will not be estimated directly, but its effect will be included in the lateral displacement u.

$$I_2(\alpha x + \tau, y + u) = I_1(x, y) \tag{2}$$

Among the three parameters describing the image deformation, only two are independent. Indeed, the axial shift τ results from the accumulation of the axial compressions (represented by α) of ROIs located between the probe and the current investigated region. By adopting an adequate strategy to displace the ROI, from the probe downwards, τ will be deduced from the previously estimated α.

The technique we developed (Fig.2) first provides an initial estimation of optimal parameters. They are determined as the arguments that maximize a similarity criterion between a specific ROI R_1 and its deformed version, when the latter is compensated for according to these parameters. The similarity criterion we chose is the normalized correlation coefficient (NCC) because it also provides information on the result's reliability. A NCC close to 1 indicates high confidence in the estimation. Moreover, because in elastography a small compression is applied to the tissue, resulting in expected small ranges for the parameter's feasible values, we used constrained optimization which increases the estimation's robustness. In terms of minimization, the problem to solve can be

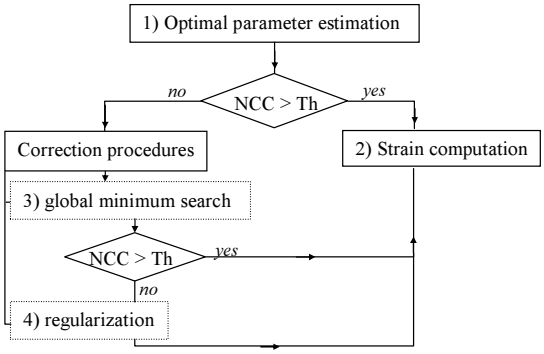

Fig. 2. Method overview.

written:

$$[\hat{\alpha}, \hat{u}] = \arg\min_{\alpha,u}[-f(\alpha, u)] \tag{3}$$
$$\alpha_{min} \leq \alpha \leq \alpha_{max}$$
$$u_{min} \leq u \leq u_{max}$$

with:

$$f(\alpha, u) = \frac{\sum(R_1(x,y) - \overline{R_1}(x,y))(R_2(\frac{x}{\alpha}, y+u) - \overline{R_2}(\frac{x}{\alpha}, y+u))}{\sqrt{\sum(R_1(x,y) - \overline{R_1}(x,y))^2 \cdot \sum(R_2(\frac{x}{\alpha}, y+u) - \overline{R_2}(\frac{x}{\alpha}, y+u))^2}} \tag{4}$$

where f is the NCC function. Equation (3) is solved using the sequential quadratic programming (SQP) methodology [8]. Such methods can be viewed as the natural extension of Newton (or quasi-Newton) techniques to the constrained optimization setting. This iterative procedure consists in modeling the defined problem at a given approximate solution by a quadratic programming (QP) subproblem and in using the QP solution as the descent direction to construct a better approximation. Once the parameters are estimated, the NCC value at the solution is considered. If it is higher than a threshold, Th, the estimation is considered reliable and the axial strain ϵ is computed:

$$\widehat{\epsilon} = \widehat{\alpha} - 1 \tag{5}$$

Otherwise, the algorithm goes through correction procedures. Given that SQP methods are only guaranteed to find a local solution of (3), the first procedure consists in initializing Nb new minimization processes from Nb points uniformly spread within the parameter domain. Indeed, an initialization close to the global minimum makes the algorithm converge towards the solution sought. The parameter vector retained is the one leading to the highest NCC. If this one is higher than Th, the axial strain is then computed. Otherwise the parameter vector is computed anew by ensuring continuity with reliable parameter vectors located in the neighborhood (Fig. 2).

3. RESULTS

Our method was tested with image sets from an elastography-dedicated phantom, as well as natural (noninduced) dog tu-

mor lesions. During experiments, the compression was applied with the probe in a freehand configuration. While the operator was slowly compressing the medium, RF images were acquired in real time ($\sim$ 25 images/sec.), with an Ultrasonix ultrasound scanner. The central and sampling frequencies were around 7 and 40 MHz, respectively.
All strain images, also termed elastograms, were computed off line using the same method parameters: R_1 measures 1.3 mm (axially) x 1.1 mm (laterally). It is displaced regularly in I_1 with an axial overlap of 75% and a lateral overlap of 60%. The bounds values for the axial scaling factors are $\alpha_{min} = 0.9$ (maximal compression) and $\alpha_{max} = 1$ (no compression). Lateral displacement bounds are chosen such that a maximum displacement of 0.7 mm on the left or on the right is allowed. Finally, Th has been set at 0.8.

3.1. Results with the CIRS elasticity phantom, model 049

The CIRS phantom, model 049, is a test object dedicated to elastographic experiments. This phantom consists of a background medium, within which are embedded eight spheres whose size, location and hardness are provided by the manufacturer. We investigated the deformation of a 10-mm-diameter sphere located at 15-mm depth. This spherical inclusion has a reported Young modulus of 54 KPa and is harder than the surrounding material whose Young modulus is 29 KPa. Figure 3a shows the conventional ultrasound B-mode image of the considered phantom section and Fig. 3b provides four elastograms extracted from the sequence of estimated strain maps at four different time points. These results demonstrate that elastography provides information that is complementary to ultrasound imaging. Whereas the inclusion is hardly detectable in the B-mode image, it is clearly brought out in the elastograms. Moreover, as expected, the harder inclusion deforms less than the surrounding material and the mean strain increases with compression, enhancing the contrast between the lesion and the background material.

3.2. Results with a dog liver tumor

The results presented in this section were obtained with a freshly excised dog liver, presenting a noninduced (natural) tumor lesion (Fig. 4a). In the ultrasound B-mode image, the lesion is characterized by an echoic core surrounded by a hypoechoic zone (Fig. 4b) with unclear borders. Figure 4c provides four elastograms extracted from the sequence of estimated strain maps during compression. The tumor lesion appears harder than the surrounding healthy tissues, with clearly defined borders and with contrast increasing with compression. Moreover, we can observe that the area of healthy tissues just above the tumor is highly strained, as expected.

3.3. Results with dog spleen tumors

Finally, the technique was used to investigate a dog spleen, characterized by the presence of multiple nodules, with and without well-identified borders.

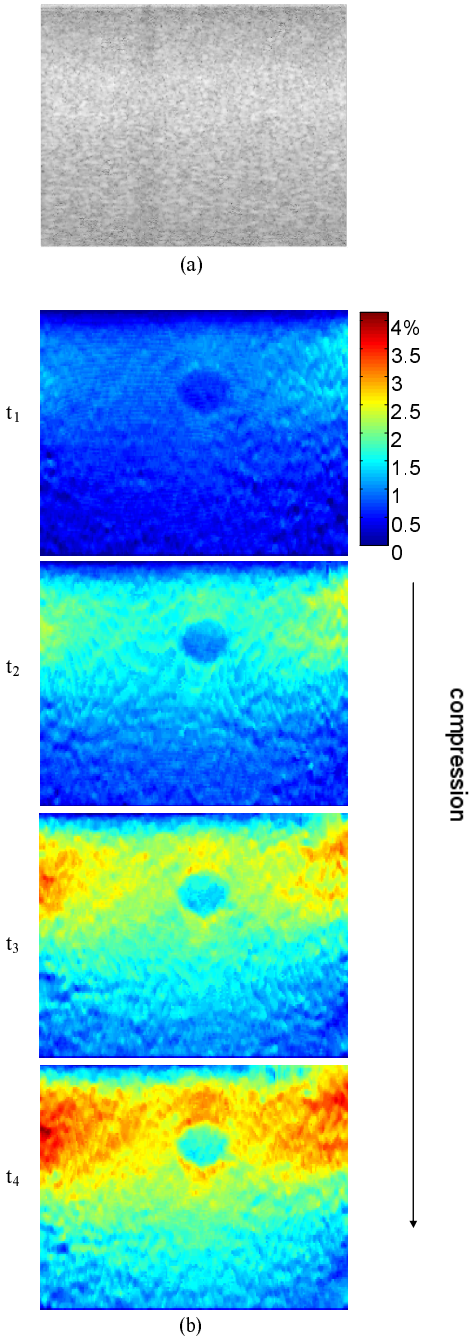

Fig. 3. (a) Conventional ultrasound B-mode image of the phantom section. (b) Evolution of the medium deformation with increasing compression. Whereas the inclusion is hardly detectable in the B-mode image, it is clearly brougth out in the elastograms.
Note: with the convention used in (5), the strain is negative for a compression and positive for a dilatation. Since in elastography a compression is applied to the tissue, the strains are all negative. For simplification purposes the opposite of the strain is shown.

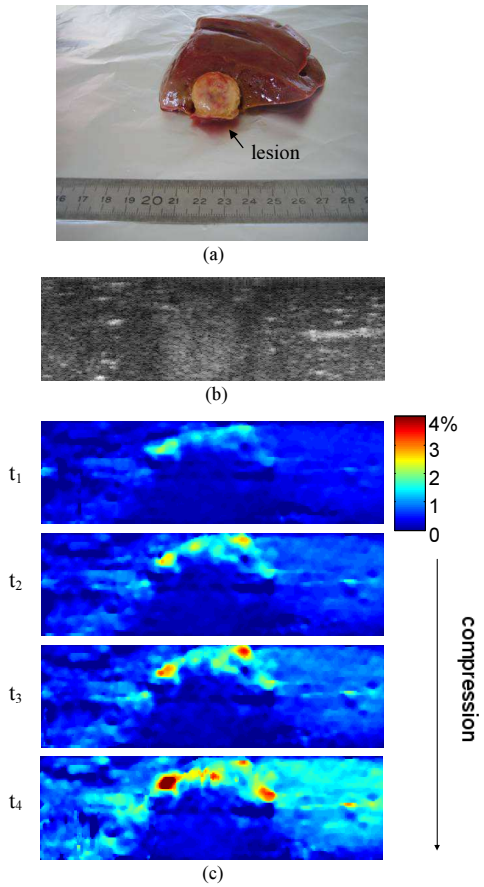

Fig. 4. (a) Photograph of the dog liver sample. (b) Conventional ultrasound B-mode image. (c) Deformation images with the compression for four time points. The lesion is clearly brought out in the elastograms with sharp boundaries.

The ultrasound image as well as four elastograms obtained during compression are presented in Fig.5a and 5b, respectively. It can be seen that strain images provide information that is complementary to the B-mode image. Indeed, in Fig. 5a, essentially two tumor areas are visible (numbered 1 and 2 in Fig. 5b). In the elastograms, these areas appear harder with clearly delineated boundaries. Moreover, the elastograms show a third lesion (#3), very close to the lesion #2 but distinct from the latter, whereas in the ultrasound image, these two lesions seem to merge. Finally, the area #4 remains the most difficult to interpret since there is some variation in strain but no areas with sharp boundaries. Besides, no specific structure is visible in the B-mode image.

4. CONCLUSIONS AND FUTURE WORK

In this paper, a 2D locally regularized strain estimation technique has been presented and used to image the deformation of dog tissues with tumor(s) during freehand scanning. The initial results are very encouraging. Future work will focus on continuing the animal study with *in vitro* and *in vivo* experiments.

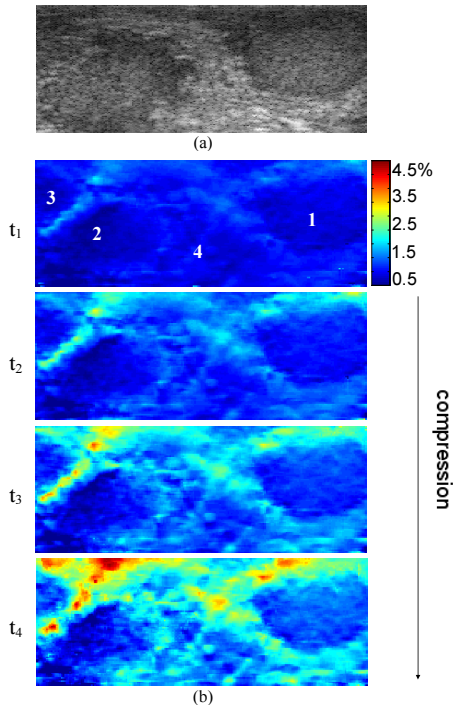

Fig. 5. (a) Ultrasound B-mode image of the dog spleen with tumors. (b) Deformation images with the compression for four time points.

4. REFERENCES

[1] J. Ophir, I. Cespedes, H. Ponnekanti, Y. Yazdi and X. Li, Elastography : a quantitative method for imaging the elasticity of biological tissues, *Ultrason. Imag.*, 13:111-134, 1991.

[2] T.A. Krouskop, T.M. Wheeler, F. Kallel, B.S. Garra, and T. Hall, Elastic Moduli of Breast and Prostate Tissues under Compression, *Ultrason. Imag.*, 20:260-274, 1998.

[3] X. Chen, M. J. Zohdy, S. Y. Emelianov and M. O'Donnell, Lateral speckle tracking using synthetic lateral phase, *IEEE UFFC*, 51(5):540-550, 2004.

[4] C. Pellot-Barakat, F. Frouin, M.F. Insana and A. Herment, Ultrasound elastography based on multiscale estimations of regularized displacement fields, *IEEE TMI*, 23(2):153-63, 2004.

[5] M. Bilgen and M. F. Insana, "Deformation models and correlation analysis in elastography", *JASA*, 99(5):3212-3224, 1996.

[6] R. L. Maurice, J. Ohayon, Y. Fretigny, M. Bertrand, G. Soulez and G. Cloutier, Noninvasive Vascular Elastography: Theoretical Framework, *IEEE TMI*, 23(2):164-180, 2004.

[7] E. Brusseau, J. Kybic, J.F. Deprez and O. Basset, 2D locally regularized tissue strain estimation from radio-frequency ultrasound images : Theoretical developments and results on experimental data, *IEEE TMI*, 27(2):145-160, 2008.